Estimates of lateral and longitudinal bond energies within the microtubule lattice

Vincent VanBuren[†‡], David J. Odde[§], and Lynne Cassimeris[†¶]

[†]Department of Biological Sciences, Lehigh University, 111 Research Drive, Bethlehem, PA 18015; and [§]Department of Biomedical Engineering, University of Minnesota, 312 Church Street, SE, Minneapolis, MN 55455

Edited by Thomas D. Pollard, Yale University, New Haven, CT, and approved March 11, 2002 (received for review September 25, 2001)

We developed a stochastic model of microtubule (MT) assembly dynamics that estimates tubulin–tubulin bond energies, mechanical energy stored in the lattice dimers, and the size of the tubulin-GTP cap at MT tips. First, a simple assembly/disassembly state model was used to screen possible combinations of lateral bond energy (ΔG_{Lat}) and longitudinal bond energy (ΔG_{Long}) plus the free energy of immobilizing a dimer in the MT lattice (ΔG_S) for rates of MT growth and shortening measured experimentally. This analysis predicts ΔG_{Lat} in the range of -3.2 to -5.7 k_BT and ΔG_{Long} plus ΔG_S in the range of -6.8 to -9.4 k_BT. Based on these estimates, the energy of conformational stress for a single tubulin-GDP dimer in the lattice is 2.1–2.5 k_BT. Second, we studied how tubulin-GTP cap size fluctuates with different hydrolysis rules and show that a mechanism of directly coupling subunit addition to hydrolysis fails to support MT growth, whereas a finite hydrolysis rate allows growth. By adding rules to mimic the mechanical constraints present at the MT tip, the model generates tubulin-GTP caps similar in size to experimental estimates. Finally, by combining assembly/disassembly and cap dynamics, we generate MT dynamic instability with rates and transition frequencies similar to those measured experimentally. Our model serves as a platform to examine GTP-cap dynamics and allows predictions of how MT-associated proteins and other effectors alter the energetics of MT assembly.

Microtubule (MT) dynamic instability plays a critical role in chromosome movement and separation during mitosis. MTs grow, shorten, and transition between these states at rates governed by the presence of various MT effectors, such as divalent cations, MT-associated proteins (MAPs), and drugs such as Taxol (1).

MTs are composed of heterodimer subunits of α- and β-tubulin. A guanine nucleotide (GTP or GDP) is positioned on the β monomer opposite the interface between the two monomers, where it is hydrolyzable (if it is GTP) and exchangeable. The β monomer end of the dimer faces the (+) end of the MT, which is the end of more active dynamics and kinetochore attachment during cell division. The α monomer faces the (−) end of the MT, which originates at the centrosome. MTs are thought to transition from a state of growth to a state of rapid shortening, termed a ''catastrophe'', when the tubulin-GTP ''cap'' is stochastically lost from the tip of the MT. The tubulin-GTP cap must exist because it has been demonstrated that tubulin-GTP subunits are added to the ends during assembly. A tubulin-GTP cap, however, has not been detected in experiments with porcine brain tubulin, and therefore must be small. Experiments suggest that the cap must be less than ≈200 dimers (2–4). Presumably, the transition from rapid shortening to growth, termed ''rescue,'' occurs when the tubulin-GTP cap is reestablished.

Interactions at the surfaces of adjacent dimers occur through discrete lateral and longitudinal noncovalent bonds. Thermodynamic studies of MT assembly are unable to quantify the energy of these lateral and longitudinal tubulin–tubulin interactions. Previous efforts to model MT assembly have used arbitrary energies for these interactions. We developed an approach to estimate bond energies by using Monte Carlo simulations of assembly and disassembly. ΔG_S gives a measure of the entropic cost of ''freezing'' a free dimer into a relatively static position in the MT lattice. Possible values for lateral bond energy (ΔG_{Lat}) and longitudinal bond energy (ΔG_{Long}) plus the free energy of immobilizing a dimer in the MT lattice (ΔG_S) were screened to find the resultant rate of growth or shortening for a given pair of values. Taking published growth rates for MTs assembled *in vitro*, we could then estimate lateral and longitudinal bond strength in the MT.

Structural features of the hollow, 13-protofilament MT likely contribute significantly to the transitions of dynamic instability. Electron micrographs reveal that disassembly occurs as protofilaments peel into ''ram's horn'' formations under high magnesium buffer conditions, or into frayed ends under physiological concentrations of magnesium (5). It is likely that mechanical stress caused by transition from conformationally straight tubulin-GTP to kinked tubulin-GDP destabilizes lateral bonds. By implementing a hydrolysis rule with a finite rate constant and by incorporating this mechanical feature, we developed a model for transitions between energetic states of MT growth and shortening. By combining the assembly/disassembly state model with rules for GTP hydrolysis, we constructed an effective model of dynamic instability that is useful for better understanding molecular events at MT tips and for predicting how interactions between tubulin dimers are altered by effectors of MT dynamic instability.

Methods

The Model. The predominant 13-protofilament B-lattice MT, assumed in the model, has a helical pitch of 3 monomers per turn of the helix (a 13_3 lattice) and a ''seam'' of neighboring interactions (α–β and β–α) that differs from the majority of neighboring interactions (α–α and β–β). In a 13_3 lattice, a given dimer may have a neighbor, half of a neighbor (at the seam), or no neighbor on each side. The α/β tubulin heterodimers are represented as dimensionless occupants of a matrix in this model. The first and last columns of this matrix are treated as neighbors, with the rows of one of the columns offset to account for interactions at the seam (Fig. 1*A*).

Previous experiments by others have shown that 1–5 $\mu M^{-1}\,s^{-1}$ is a reasonable range for the on rate of tubulin dimers (6, 7). Others have used 2 $\mu M^{-1}\,s^{-1}$ and 4 $\mu M^{-1}\,s^{-1}$ in simulations (8–10), therefore we ran parallel experiments at each of these rates to predict bond energetics. On rates [$k_{(+)}$] for each of the

This paper was submitted directly (Track II) to the PNAS office.

Abbreviations: ΔG_{Lat}, lateral bond energy between tubulin dimers; ΔG_{Long}, longitudinal bond energy between tubulin dimers; ΔG_S, free energy of immobilizing a dimer in the MT lattice; $\Delta G^{\ddagger}_{Long}$, $\Delta G_{Long} + \Delta G_S$; ΔG_{Kink}, mechanical potential energy of a tubulin-GDP held in an unrelaxed straight conformation; MT, microtubule; MAP, MT-associated protein.

[‡]Present address: Laboratory of Genetics, National Institute on Aging, Baltimore, MD 21224.

[¶]To whom reprint requests should be addressed. E-mail: lc07@lehigh.edu.

The publication costs of this article were defrayed in part by page charge payment. This article must therefore be hereby marked "*advertisement*" in accordance with 18 U.S.C. §1734 solely to indicate this fact.

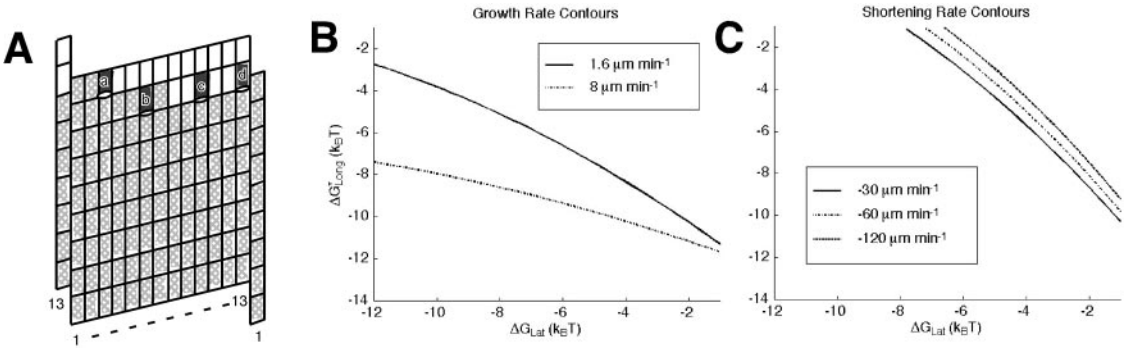

Fig. 1. (*A*) Diagram of the matrix used in modeling and examples of possible binding sites. The hollow MT is simulated by the contact between the first and last columns of the matrix with columns offset to mimic interactions at the seam. Filled sites in the matrix are crosshatched. Potential binding sites for incoming dimers have one longitudinal bond (white ellipse). Sites may have a variable number of lateral bonds: 1 (a), 2 (b), 0 (c), or 0.5 (d). Bond energy is summed and the result is used to calculate k_{off} at that site (see text). (*B* and *C*) Predicted net growth rate as a function of ΔG^*_{Long} and ΔG_{Lat}. Contours were plotted to visualize the energy curves for experimentally observed growth or shortening rates at $k_{(+)} = 4\ \mu M^{-1}\,s^{-1}$. Assembly rates (*B*) and disassembly rates (*C*) are shown as separate plots for clarity. No GTPase activity is postulated here.

13 association sites at the MT tip are equal and remain constant. If $k_{(+)}$ is held constant, then differences in kinetics must result from differences in $k_{(-)}$. Differences in $k_{(-)}$ arise from the presence or absence of neighbors and from the state of the dimer in question (tubulin-GTP or tubulin-GDP).

Simulation Procedure. We use the simplification that all dimers recruited to bind to the MT have at least one longitudinal bond. As there is also one term for each dimer describing the energy of immobilization (ΔG_S), we may treat ΔG_{Long} and ΔG_S collectively: $\Delta G^*_{Long} = \Delta G_{Long} + \Delta G_S$. We are then not required to use a separate estimate for ΔG_S, and thus maintain a simple parameter set. Total bond energy depends on the number of lateral bonds (ΔG_{Lat}), which varies from dimer to dimer.

Hill (11) showed that the equilibrium constant (K) and the free energy change (ΔG) of polymerization are related by the equation:

$$\Delta G = -k_B T \ln(K[\text{tubulin-GTP}]), \qquad [1]$$

where k_B is Boltzmann's constant, T is the absolute temperature of the reaction (K) (for molar quantities at 37°C, 1 k_BT converts to ≈0.6 kcal mol^{-1}), and K is the equilibrium constant (M^{-1}) given by:

$$K = \frac{k_{(+)}}{k_{(-)}}, \qquad [2]$$

where $k_{(+)}$ is the bimolecular on rate constant ($M^{-1}\,s^{-1}$) and $k_{(-)}$ is the unimolecular off rate (s^{-1}).

Each round of simulations begins with the formulation of a list of possible events, including one possible association event for each protofilament and one possible dissociation event for each dimer in the entire lattice. We use the following rule for dissociation events: when a dimer dissociates, all dimers above it (toward the active tip) in the same protofilament also dissociate. The total energy of all of the above lateral bonds (ΔG_{Lat}) is summed together with the total ΔG_{Lat} and ΔG^*_{Long} of the dimer under consideration to calculate $k_{(-)}$. In practice, this makes dissociation of a dimer buried more than a few layers deep a very rare event.

The rate of each item in the list is determined as follows: $k_{(+)}$ is assigned a single value, and thus all association events have an equal rate at constant free tubulin concentration. The rate constant $k_{(-)}$ is determined by first summing all of the energies (ΔG_{Lat} and ΔG^*_{Long}) that would be lost through dissociation to get ΔG, then solving for K in Eq. **1** and combining it with the assigned value for $k_{(+)}$; $k_{(-)}$ may then be computed with Eq. **2**. In a model that merges the results of our assembly and disassembly state models, a hydrolysis event is added to the list of possible events for each unhydrolyzed dimer below the endmost dimer, where hydrolysis may be thought of as changing a particular tubulin dimer from the "assembly state" to the "disassembly state." Hydrolysis rates are assigned in these experiments.

Next, a random number from 0 to 1 is generated for each item in the event list. This number is used in the following equation to obtain a single realization of the exponentially distributed time required for each possible event:

$$t_i = \frac{-\ln(R_i)}{k_i}, \qquad [3]$$

where i is the index of the possible event, k is the first-order rate constant of the event (s^{-1}), R is a uniformly distributed, uncorrelated random number chosen from the interval 0–1, and t is the resulting execution time that the ith event requires (s) (10, 12, 13). The final step in each iteration is to choose the member of the event list that has the shortest execution time, as calculated with Eq. **3**. The event having the shortest execution time is implemented, and the total elapsed time is updated.

Simulations. To create contour graphs with assembly velocity as a function of ΔG_{Lat} and ΔG^*_{Long}, simulations were run over the range -1 to $-20\ k_BT$ for both ΔG_{Lat} and ΔG^*_{Long} (at 0.5 k_BT intervals), assuming a 10 μM free tubulin-GTP concentration. Four trials were averaged at each point for a growth velocity estimation, for a total of 6,084 simulations; 500 events (total of association and dissociation events) were performed in each simulation. This series of simulations was repeated for a smaller range of binding energies at tubulin-GTP concentrations of 5, 15, and 20 μM. Contours were fit to second-order polynomials for curve-smoothing.

To predict a hydrolysis rate that would produce observed transition frequencies, 30 simulations were averaged to produce each mean time to catastrophe or rescue. Catastrophe frequency simulations began with an MT capped by 4 GTP-tubulin layers (52 dimers) and ran until the GTP-cap size (number of tubulin-GTP dimers) was zero. Experiments by Caplow and Shanks (14) suggested that <13 tubulin-GTP dimers at a MT tip would result in catastrophe. Here we used complete loss of the GTP cap as a convenient way to mark a catastrophe. In our simulations it is rare for a GTP cap to dip below 13 tubulin-GTPs without proceeding to catastrophe, thus our simple definition of catas-

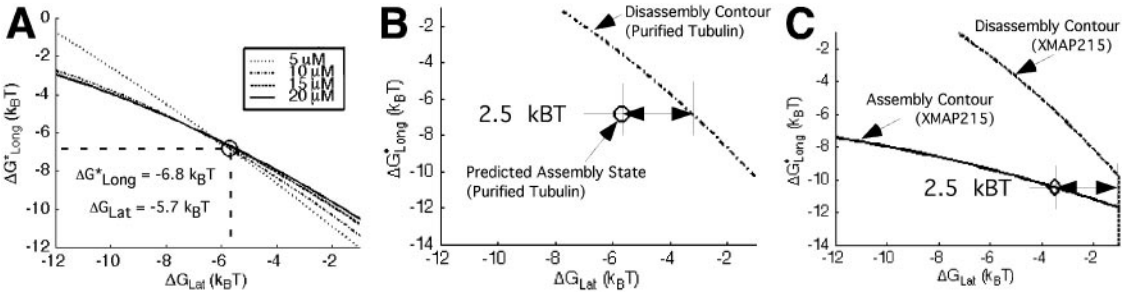

Fig. 2. Estimation of $\Delta G^{*}_{\mathrm{Long}}$ and ΔG_{Lat} by comparison to published growth rate data. (*A*) Simulations were run at tubulin concentrations of 5, 10, 15, and 20 μM [$k_{(+)} = 4\ \mu\mathrm{M}^{-1}\ \mathrm{s}^{-1}$]. Contour lines were plotted at experimentally observed rates of assembly for each concentration. The point where the lines intersect yields unique parameter values. (*B*) Prediction of ΔG_{Kink}. The values for ΔG_{Lat} and $\Delta G^{*}_{\mathrm{Long}}$ at $k_{(+)} = 4\ \mu\mathrm{M}^{-1}\ \mathrm{s}^{-1}$ are indicated with a circle. ΔG_{Kink} is predicted to be 2.5 $k_{\mathrm{B}}T$ by measuring the lateral energy change ($\Delta\Delta G_{\mathrm{Lat}}$, double arrow) from the circle to the contour for observed disassembly ($-30\ \mu\mathrm{m\ min}^{-1}$). (*C*) The energetic change that XMAP215 generates is predicted by finding the point (diamond) on the XMAP215 assembly contour ($8\ \mu\mathrm{m\ min}^{-1}$) that measures an energetic distance equal to ΔG_{Kink} (double arrow, 2.5 $k_{\mathrm{B}}T$) from the XMAP215 disassembly contour ($-60\ \mu\mathrm{m\ min}^{-1}$). Polynomials fit poorly for $\Delta G_{\mathrm{Lat}} > -1\ k_{\mathrm{B}}T$, therefore these coordinates were not plotted. Real contours that reach $\Delta G_{\mathrm{Lat}} = -1\ k_{\mathrm{B}}T$ turn sharply and follow closely along $\Delta G_{\mathrm{Lat}} = -1\ k_{\mathrm{B}}T$, thus where $\Delta G_{\mathrm{Lat}} > -1\ k_{\mathrm{B}}T$, the contour for $\mathrm{V_{rs}} = -60\ \mu\mathrm{m\ min}^{-1}$ is estimated to follow along $\Delta G_{\mathrm{Lat}} = -1\ k_{\mathrm{B}}T$ for our XMAP215 predictions.

trophe is consistent with experimental estimates of the minimal size of a stabilizing cap. Rescue frequency simulations began with an uncapped MT and ran until the MT cap was nonzero for 5 continuous seconds. Rescue occurrence was marked at the beginning of the 5 sec of nonzero cap size. Cap-size measurements were taken from single simulations run for 2 min of simulation time for each point plotted. Data for dilution experiments were collected by averaging 30 simulations for each point graphed. Error bars give SDs.

Results

Estimation of Lateral and Longitudinal Association Energies for Dimers Within the MT Lattice. The results of Monte Carlo modeling for growing or shortening MTs have been plotted as contour lines in which each line represents all possible combinations of ΔG_{Lat} and $\Delta G^{*}_{\mathrm{Long}}$ capable of generating a specific growth or shortening velocity (Fig. 1 *B* and *C*). To estimate the actual values for ΔG_{Lat} and $\Delta G^{*}_{\mathrm{Long}}$, we ran (+) end simulations at 5, 10, 15, and 20 μM tubulin. For each set of simulations, a contour was plotted at the rate of assembly measured for porcine tubulin (data from ref. 15). The energy values should not be concentration-dependent, therefore these contours should intersect at a point that represents the predicted value of ΔG_{Lat} and $\Delta G^{*}_{\mathrm{Long}}$ for tubulin dimers within the MT. At $k_{(+)} = 2\ \mu\mathrm{M}^{-1}\ \mathrm{s}^{-1}$, the model predicts ΔG_{Lat} is $-3.2\ k_{\mathrm{B}}T$ and $\Delta G^{*}_{\mathrm{Long}}$ is $-9.4\ k_{\mathrm{B}}T$ (not shown). At $\mathrm{k_{(+)}} = 4\ \mu\mathrm{M}^{-1}\ \mathrm{s}^{-1}$, the model predicts ΔG_{Lat} is $-5.7\ k_{\mathrm{B}}T$ and $\Delta G^{*}_{\mathrm{Long}}$ is $-6.8\ k_{\mathrm{B}}T$ (Fig. 2*A*).

The observed rate of rapid shortening of MTs is $\approx -30\ \mu\mathrm{m\ min}^{-1}$ and the fastest observed shortening occurs at $\approx -120\ \mu\mathrm{m\ min}^{-1}$ in buffers containing high concentrations of magnesium ions (16). Shortening-rate contours in the -30 to $-120\ \mu\mathrm{m\ min}^{-1}$ range are within $\approx 1\ k_{\mathrm{B}}T$ of each other, suggesting that the 4-fold increase in shortening rate caused by high magnesium requires only a $\approx 1\ k_{\mathrm{B}}T$ difference in the sum of a single lateral interaction and a single longitudinal interaction (Fig. 1*C*). The model predicts that large differences in disassembly rates may be governed by small changes in bond energetics.

Prediction of Potential Mechanical Energy of a GDP-Tubulin Within the MT Lattice. Our model for (+) end assembly and disassembly may be considered a state model, in which moving from one state to another is the same as moving from one energy contour to another. The coordinates predicted above for basal ΔG_{Lat} and $\Delta G^{*}_{\mathrm{Long}}$ are a starting point from which other states (contours) may be reached by altering these energies. The assembly state is associated with the presence of tubulin-GTP at the tip of the MT, and the disassembly state is associated with the presence of tubulin-GDP at the MT tip, therefore the difference in energies between the two states may be regarded as the change in tubulin–tubulin interaction.

Kinking energy (ΔG_{Kink}), the potential mechanical energy of a tubulin-GDP held in an unrelaxed straight conformation, was estimated by applying graphical analysis to our state model for MT assembly. ΔG_{Kink} should destabilize lateral bonds, therefore we estimated ΔG_{Kink} by measuring the energetic change necessary to step from the predicted energy coordinates for assembly (Fig. 2*A*) to a disassembly contour ($-30\ \mu\mathrm{m\ min}^{-1}$, 10 μM tubulin-GTP) by altering only ΔG_{Lat} (i.e., using only a change along the *x* axis). We estimated ΔG_{Kink} to be 2.1 $k_{\mathrm{B}}T$ at $\mathrm{k_{(+)}} = 2\ \mu\mathrm{M}^{-1}\ \mathrm{s}^{-1}$ (not shown) and 2.5 $k_{\mathrm{B}}T$ at $\mathrm{k_{(+)}} = 4\ \mu\mathrm{M}^{-1}\ \mathrm{s}^{-1}$ (Fig. 2*B*).

XMAP215 Is Predicted to Increase the Apparent Strength of Longitudinal Interactions. The model can be used to predict the energetic changes caused by MT binding proteins. For example, we used this simple Monte Carlo model to examine how XMAP215 can cause both a $\approx$7-fold increase in the growth rate and a $\approx$3-fold increase in the shortening rate (17). XMAP215 causes a disassembly state change from $\mathrm{V_{rs}} = \approx -20\ \mu\mathrm{m\ min}^{-1}$ to $\mathrm{V_{rs}} = \approx -60\ \mu\mathrm{m\ min}^{-1}$, and an assembly state change from $\mathrm{V_e} = \approx 1.5\ \mu\mathrm{m\ min}^{-1}$ to $\mathrm{V_e} = \approx 8\ \mu\mathrm{m\ min}^{-1}$. Although XMAP215 will form its own bonds with MTs, it will have the apparent effect of strengthening either lateral or longitudinal tubulin–tubulin bonds, depending on the orientation of XMAP215 on the MT. Above, we predicted that the kinking energy was 2.1 $k_{\mathrm{B}}T$ for $k_{(+)} = 2\ \mu\mathrm{M}^{-1}\ \mathrm{s}^{-1}$ and 2.5 $k_{\mathrm{B}}T$ for $k_{(+)} = 4\ \mu\mathrm{M}^{-1}\ \mathrm{s}^{-1}$, which is the energy difference for lateral bonds responsible for the state change from $\mathrm{V_e} = \approx 1.5\ \mu\mathrm{m\ min}^{-1}$ to $\mathrm{V_{rs}} = \approx -30\ \mu\mathrm{m\ min}^{-1}$. The energetic difference between the states $\mathrm{V_e} = \approx 8\ \mu\mathrm{m\ min}^{-1}$ and $\mathrm{V_{rs}} = \approx -60\ \mu\mathrm{m\ min}^{-1}$ should be the same. To predict ΔG_{Lat} and $\Delta G^{*}_{\mathrm{Long}}$ with XMAP215 present, we begin our graphical analysis by drawing curves at $\mathrm{V_e} = \approx 8\ \mu\mathrm{m\ min}^{-1}$ and $\mathrm{V_{rs}} = \approx -60\ \mu\mathrm{m\ min}^{-1}$, the assembly and disassembly velocities produced by XMAP215 (Fig. 2*C*). The predicted energy states produced by XMAP215 are found by determining which points on these two curves are separated by ΔG_{Kink} [2.5 $k_{\mathrm{B}}T$ for $\mathrm{k_{(+)}} = 4\ \mu\mathrm{M}^{-1}\ \mathrm{s}^{-1}$]. This analysis reveals the only points where an energy change of ΔG_{Kink} will produce a transition from observed XMAP215 assembly to disassembly rate (Fig. 2*C*). It is estimated that in the presence of XMAP215, longitudinal bonds are apparently strengthened by 3.6 $k_{\mathrm{B}}T$ and 3.8 $k_{\mathrm{B}}T$, for $k_{(+)} = 2\ \mu\mathrm{M}^{-1}\ \mathrm{s}^{-1}$ and $k_{(+)} = 4\ \mu\mathrm{M}^{-1}\ \mathrm{s}^{-1}$, and that lateral bonds are apparently weakened by 0.2 $k_{\mathrm{B}}T$ and 2.2 $k_{\mathrm{B}}T$, for $k_{(+)} = 2\ \mu\mathrm{M}^{-1}$

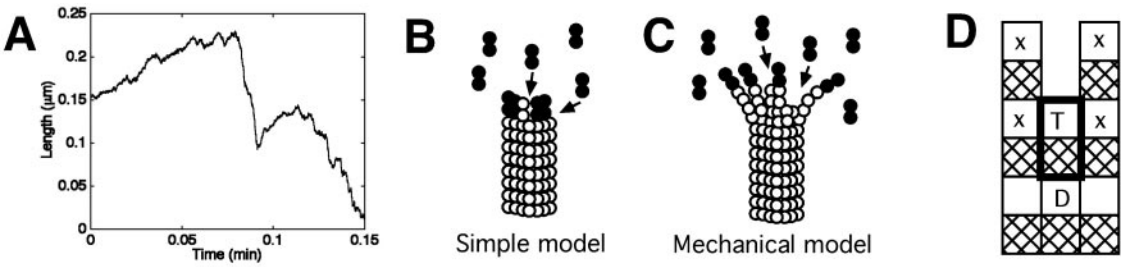

Fig. 3. Incorporation of hydrolysis and mechanics into the model. (*A*) Dynamic instability is produced with a spatially coupled, noninstantaneous hydrolysis rule, although growth and shortening phases are too brief (see text). (*B* and *C*) MT tip structures in a simple model (*B*) and in a more complete mechanical model (*C*). A simple model cannot accurately describe rescue from disassembly because GTP-tubulin association stabilizes ends and rescues occur too frequently (*B*). A mechanical model would represent rescues more accurately by reducing the stabilizing effect of GTP-tubulin association at splaying tips (*C*). (*D*) Modification of the simple model to incorporate mechanical effects. If a tubulin-GTP dimer associates at a position above a tubulin-GDP, the incoming dimer is ''tagged'' and its energetics are treated as though it is a tubulin-GDP to mimic the mechanical situation illustrated in *C*. Tagged tubulin-GTP may regain its proper energetic state if two of four nearby positions (x) are occupied by tubulin-GTP.

s^{-1} and $k_{(+)} = 4\ \mu M^{-1}\ s^{-1}$ [Fig. 2*C*, $k_{(+)} = 2\ \mu M^{-1}\ s^{-1}$ (not shown)].

Hydrolysis Rules. The above results modeled discrete assembly and disassembly states; to model transitions, these state models must be merged together with rules for changing the state of dimers. Based on the structure of the MT, Nogales *et al.* (18) proposed that GTP hydrolysis is coupled to subunit addition; contact between α tubulin of one subunit and β tubulin of the other catalyzes hydrolysis of the GTP between these subunits. If the catalyzed hydrolysis is very rapid, this will generate a GTP cap that is 1 subunit-deep. We tested this model by simulating MT assembly at (+) ends, using the values for ΔG_{Lat} and ΔG^*_{Long} measured above. Each simulation began in an assembly state, with a single layer of tubulin-GTP at the tip of a blunt-end MT. Under these conditions, temporally coupled hydrolysis always caused immediate (<1 sec) switching to rapid shortening (data not shown), demonstrating that an instantaneous hydrolysis rule is not viable.

Because an instantaneous coupling between subunit addition and GTP hydrolysis failed to accurately simulate MT behavior, we modeled hydrolysis as a first-order reaction with a finite rate constant, k. In this model, only dimers with at least one dimer above them are capable of undergoing hydrolysis. Addition of a dimer is still necessary to stimulate hydrolysis of the dimer below, but hydrolysis is not temporally coupled to addition. This modified hydrolysis rule allows MT assembly with sustained periods of growth. For example, at a hydrolysis rate of $10\ s^{-1}$, the model produced persistent growth with a typical time to catastrophe of about ≈5 s and a typical time to rescue of ≈1 s (Fig. 3*A*).

State Models and a Finite Rate Hydrolysis Model May Be Merged to Form a Complete Model of Dynamic Instability. Although the stochastic hydrolysis rule produced sustained periods of growth, the periods were still shorter than observed experimentally and also failed to generate rapid shortening phases similar to experimentally measured values. Rapid shortening persisted if the hydrolysis rate was raised but the MT could not maintain a significant growth phase (not shown). Electron micrographs reveal that MT tips may assume a variety of conformations, including blunt ends, sheet-like extensions, curved protofilament extensions, or splaying protofilaments (19–21). Therefore, we hypothesized that mechanical and structural features of the MT tip must be included to produce a simulation able to reproduce dynamic instability. In a mechanical model of MT disassembly, association of tubulin-GTP dimers to the tips of splaying or fraying protofilaments would have a comparatively weak stabilizing effect, as newly added dimers would not be expected to have neighbors sufficiently close for strong lateral associations (Fig. 3 *B* and *C*). We mimicked this behavior by imposing a rule that a new tubulin-GTP dimer that associates on top of a tubulin-GDP dimer should be ''tagged.'' The bond energies of the tagged dimers are then treated as though they were tubulin-GDP dimers. Tagged dimers switch back to tubulin-GTP status at (+) ends if they are stabilized by having, or by gaining, two tubulin-GTP neighbors among four possible dimer positions (Fig. 3*D*). The tagged dimers were treated normally with regard to hydrolysis, and thus could be hydrolyzed to become tubulin-GDP while tagged. This special treatment of weakly stabilizing tubulin-GTP associations allows disassembly to persist as a discrete state that is not slowed by competition with tubulin-GTP association. Tubulin-GTP association, however, is able to generate a rescue with some small probability that depends on the hydrolysis rate (see below). Minus (−) ends are modeled by using only two deviations from the methods described above for (+) ends. (*i*) Hydrolysis of terminal dimers is permitted, and (*ii*) dimers may become untagged under a more permissive rule: only one of the four positions indicated must be occupied by a tubulin-GTP for untagging (Fig. 3*D*).

The tubulin two-state model was merged with the above rules for hydrolysis, thus allowing tubulin dimers to change from GTP to GDP states. Simulations were performed over a range of hydrolysis rates (with 10 μM tubulin-GTP) to determine the mean times to catastrophe and rescue at each possible hydrolysis rate (Fig. 4*A*). Mean time to catastrophe fits a power curve and mean time to rescue is linear. The experimentally observed mean time to catastrophe (≈4 min) occurs at a hydrolysis rate constant of $\approx 0.95\ s^{-1}$. At this hydrolysis rate, the mean time to rescue is ≈0.7 min, compared with the experimentally observed value of ≈1 min. By applying a hydrolysis rate constant of $0.95\ s^{-1}$ together with our estimates for bond energies, our model reproduces dynamic instability with experimentally observed assembly and disassembly rates and transition frequencies at (+) ends (Fig. 4*B*).

The relationship of the curves describing mean times to catastrophe and rescue suggests that hydrolysis rate can have a large effect on catastrophe frequency without having a discernable effect on rescue frequency. For example, our simulations reveal that a change in hydrolysis rate from $0.95\ s^{-1}$ to $1.10\ s^{-1}$ caused about a 3-fold increase in catastrophe frequency, but caused no discernable change in rescue frequency.

The model was extended to (−) ends with the tubulin-GTP-tagging method described above. Simulations at 10 μM tubulin generated a growth rate of 1.2 μm/min and a shortening rate of 19 μm/min. Average (−) end growth time was 15 min and average shortening time was 0.01 min. In general, the (−) end simulations qualitatively reflect the differences in (+) and (−)

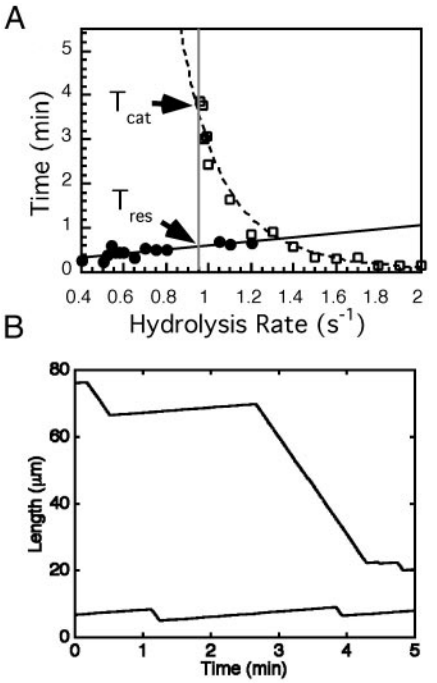

Fig. 4. A single hydrolysis rate generates both the experimentally observed mean times to both catastrophe and rescue. (*A*) Plots of mean times to catastrophe (T_{cat}) and rescue (T_{res}) vs. hydrolysis rate constant. A hydrolysis rate of ≈0.95 s^{-1} produced the experimentally observed mean times to catastrophe (≈4 min) and rescue (≈0.7 min). Adding this hydrolysis rule did not change the predictions made in Figs. 1 and 2. (*B*) Examples of life history plots at a hydrolysis rate of 0.95 $molecule^{-1}$ s^{-1}.

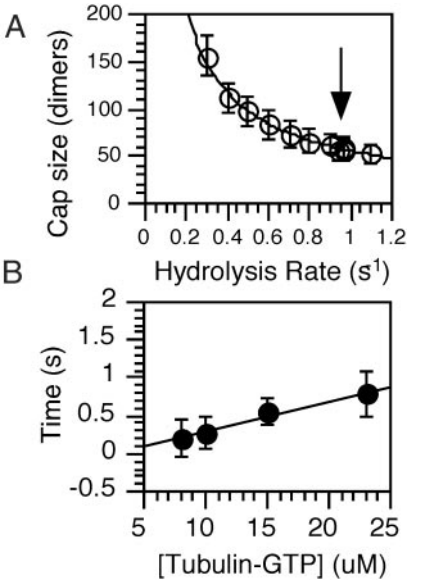

Fig. 5. Predicted tubulin-GTP cap size and dynamics. (*A*) The mean tubulin-GTP cap size depends inversely on hydrolysis rate. A hydrolysis rate constant of 0.95 $molecule^{-1}$ s^{-1} (arrow) predicts a tubulin-GTP cap size of ≈55 dimers with an SD of ≈12 dimers. (*B*) Simulated dilution of tubulin to 20% of the starting concentration results in rapid disassembly onset within ≈1 s, with only a weak correlation to the initial tubulin-GTP concentration.

end assembly dynamics measured experimentally (15). For example, simulations predicted that catastrophes were more frequent at (+) ends whereas rescues were more frequent at (−) ends. It should be noted that the rescue frequency estimated by simulation is higher than that measured experimentally. Because the present model only mimics mechanical features of the MT, it is not surprising that some deviations with experiment were observed.

GTP-Cap Size Is Regulated by Hydrolysis Rate and the Predicted Hydrolysis Rate Produces a Small Cap. Mean (+) end cap size and its SD were calculated for a range of hydrolysis rate constants from 0.3 to 1.1 s^{-1}. The hydrolysis rate constant governed the mean size of the tubulin-GTP cap and was fit to a power curve (Fig. 5*A*). Given an observed mean time to catastrophe of ≈4 min, our simulations predict a cap size of ≈55 dimers, with an SD of ≈12 dimers. A small cap size with small SD is in agreement with experimental data, as the tubulin-GTP cap must be small (<200 dimers) to have remained undetected by experiment (2–4, 14).

Dilution Produces a Fast Transition to Rapid Disassembly Over a Wide Range of Tubulin-GTP Concentrations. Simulated dilution experiments were performed to determine how the speed of rapid disassembly onset in the combined model compared with experimentally observed results (2, 3). For simulations, the initial tubulin concentration (8–23 μM) was abruptly changed to 20% of the starting concentration, as was done experimentally (2, 3). Onset of rapid disassembly was fast (<1 s) and did not correlate strongly with the tubulin concentration before dilution (R^2 = ≈0.487) (Fig. 5*B*), which agrees well with the experimental data of Voter *et al.* (2). Other experiments (3) found a longer time lag between dilution and the onset of disassembly, but this may result from time resolution limitations.

Discussion

Toward A New Model of Dynamic Instability. Tubulin and MT structural information has provided sufficient insight to design a new computer model of MT dynamics that offers significant improvements over previous models. Our model reproduces a wide range of experimental results for the (+) ends of MTs and offers aesthetic features lacking in previous models. First, our model reproduces experimental MT dynamic instability by (*i*) robustly producing MTs with experimentally observed rates of growth and shortening over a range of tubulin concentrations, (*ii*) producing MTs with the experimentally observed transition frequencies at 10 μM tubulin-GTP, (*iii*) producing MTs with experimentally undetectable GTP caps (less than ≈200 dimers), and (*iv*) producing MTs that catastrophe after dilution at the fastest rates measured experimentally. Aesthetically, the model (*i*) uses physically based parameter sets, so that alterations of parameters can be easily interpreted, and (*ii*) uses a small set of parameters, so parameter sets may be examined exhaustively. This model is useful for rapidly scanning parameter sets and making predictions about how MT effectors change the energetics of assembly. A similar approach to modeling energetics should be feasible for estimating bond strength in other systems such as actin filaments.

The model framework presented here provides insight into the energetics of MT behavior. We found that longitudinal bonds are stronger than lateral bonds. The model predicts ΔG^*_{Long} is −6.8 to −9.4 k_BT. Erickson (8) predicts ΔG_S is 11.7–18.4 k_BT. Subtracting this free energy value from our prediction gives longitudinal bond energy of −18.5 to −27.8 k_BT. We predict lateral bond energy is −3.2 to −5.7 k_BT per dimer (half this per monomer), therefore longitudinal bonds are ≈5-fold stronger. Prediction of strong longitudinal bonds and relatively weak lateral bonds is in agreement with structural observations (18). We also estimated that the potential mechanical energy of tubulin-GDP conformational stress in the MT lattice is 2.1–2.5

CELL BIOLOGY

k_BT, in approximate agreement with thermodynamic studies that suggest $\approx$2.8 k_BT per tubulin-GDP is stored in the MT lattice (14, 22, 23).

Our model satisfies GTP-cap size requirements and represents an improvement over previous models of dynamic instability. Chen and Hill (24) designed the first Monte Carlo simulation of MT dynamics that yielded a multiple-helix model of the GTP cap. In this Fluctuating Cap model, subunit addition was uncoupled from hydrolysis. A major weakness of this model was that it produced a tubulin-GTP cap that should have been experimentally detectable, sometimes hundreds of dimers in length (24). By instantaneously coupling hydrolysis to association, the Lateral Cap model succeeded in reproducing dynamic instability while maintaining a small GTP cap (9, 10, 13). The Lateral Cap model, however, has a large set of parameters and thus it is difficult to interpret the effects of changing a particular parameter in the context of the values that the other parameters may assume. The Lateral Cap model also fails to produce all observed assembly parameters with a single set of model parameters. Furthermore, the Lateral Cap model was conceived before the crystal structure of tubulin was available, and parameters were given for all possible binding relationships, including diagonal interactions that were absent from the high-resolution model of the MT (18, 25).

By using a stochastic hydrolysis rule, Flyvbjerg *et al.* (26) developed a more abstract model of MT assembly dynamics. The strength of this model is that a small parameter set predicted catastrophe frequencies with a dependence on tubulin subunit concentration similar to that measured experimentally. However, their model did not allow estimation of GTP cap size, because it did not model at the level of tubulin–tubulin interactions in the MT. Their model also could not reproduce MT rescues, because shortening MTs were allowed to persist through regions of tubulin-GTPs (26). The present model represents an improvement over the Flyvbjerg *et al.* model, because it models at the level of tubulin dimers within a MT lattice, allowing tests of molecular mechanisms responsible for catastrophe or rescue.

An infinite hydrolysis rate constant, as used in the Lateral Cap model, does not provide an MT tip structure capable of sustaining growth in our model. Using a finite hydrolysis rate constant has allowed us to generate the observed catastrophe frequency, and predicts a tubulin-GTP cap of $\approx$55 dimers. This estimate is consistent with experimental observations, suggesting that the cap must be less than 200 dimers (2–4). The size of the cap fluctuates, but does so with an SD of $\approx$12 dimers, placing the typical range at 43–67 dimers. Based on experimental evidence, Voter *et al.* (2) predicted a GTP cap size below 40 dimers at the (+) end of MTs, similar to our estimate. Modeling experiments also demonstrated that rapid disassembly began quickly after dilution, consistent with the fastest times determined by experiment (<1 s) (2). Depolymerization onset also did not depend on the predilution tubulin concentration, as also measured experimentally (2).

The model is a useful tool for investigating the energetic effects of agents that bind MTs and alter dynamic instability parameters. For example, the results suggest that XMAP215 increases the apparent strength of longitudinal bonds, consistent with data suggesting that XMAP215 binds along a protofilament (27). The energy predictions also suggest that XMAP215 binding may weaken lateral bonds. These two predictions fit a physical model in which XMAP215 binds along a protofilament, thus increasing apparent longitudinal bond strength and possibly stabilizing the curved conformation of peeling protofilaments, antagonizing lateral bonds. It should be possible to apply this model to make predictions for the energetics of many effectors of MT dynamic instability similar to our approach with XMAP215.

Limitations of the Model and Future Work

Although our model is able to make predictions of lateral and longitudinal binding energies, these predictions are sensitive to the value chosen for $k_{(+)}$. The expected range of possible values for the $k_{(+)}$ of tubulin-GTP, 1–5 $\mu M^{-1}\,s^{-1}$, may be narrowed by assessing $k_{(+)}$ with molecular dynamics simulations. A further shortcoming of the model is that it produces growth lifetimes that more steeply depend on tubulin-GTP concentration than that observed (not shown), suggesting that a mechanical model may be necessary to better represent MT state transitions.

Accounting for mechanical features is a key feature of our model that was absent in previous models. A model that gives a fuller treatment of MT mechanics is required to understand how the energetics of dimer kinking might specifically affect the binding properties of neighbors. This mechanical model will be computationally time-consuming and therefore will be difficult to use in exhaustive trials of parameter sets. Our simplified mechanical model of MT dynamics will serve as a framework to better define parameter sets, which can then be applied to a more complete mechanical model.

We are grateful to Bob Skibbens for use of his computer facilities. Thanks to Victor Barocas and Konstantin Zalutsky for useful discussions on computational procedures. This work was supported by National Institutes of Health Grant GM58025 (to L.C.), by National Science Foundation Grant BES 9984955 (to D.J.O.), and by a Whitaker Foundation Biomedical Engineering Research grant (to D.J.O.). V.V. was supported by a fellowship from Aventis Pharmaceuticals (Bridgewater, NJ).

1. Desai, A. & Mitchison, T. (1997) *Annu. Rev. Cell Dev. Biol.* **13,** 83–117.
2. Voter, W. A., O'Brien, E. T. & Erickson, H. P. (1991) *Cell Motil. Cytoskeleton* **18,** 55–62.
3. Walker, R. A., Pryer, N. K. & Salmon, E. D. (1991) *J. Cell Biol.* **114,** 73–81.
4. Drechsel, D. N. & Kirschner, M. W. (1994) *Curr. Biol.* **4,** 1053–1061.
5. Mandelkow, E. M., Mandelkow, E. & Milligan, R. A. (1991) *J. Cell Biol.* **114,** 977–991.
6. Koren, R. & Hammes, G. G. (1976) *Biochemistry* **15,** 1165–1171.
7. Northrup, S. H. & Erickson, H. P. (1992) *Proc. Natl. Acad. Sci. USA* **89,** 3338–3342.
8. Erickson, H. P. (1989) *J. Mol. Biol.* **206,** 465–474.
9. Bayley, P., Schilstra, M. & Martin, S. (1989) *FEBS Lett.* **259,** 181–184.
10. Martin, S. R., Schlistra, M. J. & Bayley, P. M. (1993) *Biophys. J.* **65,** 578–596.
11. Hill, T. L. (1985) *Proc. Natl. Acad. Sci. USA* **82,** 4404–4408.
12. Kleutsch, B. & Freland, E. (1991) *Eur. Biophys. J.* **19,** 203–211.
13. Bayley, P. M., Schilstra, M. J. & Martin, S. R. (1990) *J. Cell Sci.* **95,** 33–48.
14. Caplow, M. & Shanks, J. (1996) *Mol. Biol. Cell* **7,** 663–675.
15. Walker, R. A., O'Brien, E. T., Pryer, N. K., Soboeiro, M. F., Voter, W. A., Erickson, H. P. & Salmon, E. D. (1988) *J. Cell Biol.* **107,** 1437–1448.
16. O'Brien, E. T., Salmon, E. D. & Erickson, H. P. (1997) *Cell Motil. Cytoskeleton* **36,** 125–135.
17. Vasquez, R. J., Gard, D. L. & Cassimeris, L. (1994) *J. Cell Biol.* **127,** 985–993.
18. Nogales, E., Whittaker, M., Milligan, R. A. & Downing, K. H. (1999) *Cell* **96,** 79–88.
19. Chretien, D., Fuller, S. D. & Karsenti, E. (1995) *J. Cell Biol.* **129,** 1311–1328.
20. Muller-Reichert, T., Chretien, D., Severin, F. & Hyman, A. A. (1998) *Proc. Natl. Acad. Sci. USA* **95,** 3661–3666.
21. Janosi, I. M., Chretien, D. & Flyvbjerg, H. (1998) *Eur. Biophys. J.* **27,** 501–513.
22. Stewart, R. J., Farrell, K. W. & Wilson, L. (1990) *Biochemistry* **29,** 6489–6498.
23. Caplow, M., Ruhlen, R. L. & Shanks, J. (1994) *J. Cell Biol.* **127,** 779–788.
24. Chen, Y. D. & Hill, T. L. (1985) *Proc. Natl. Acad. Sci. USA* **82,** 1131–1135.
25. Nogales, E., Wolf, S. G. & Downing, K. H. (1998) *Nature (London)* **391,** 199–203.
26. Flyvbjerg, H., Holy, T. E. & Leibler, S. (1996) *Phys. Rev. E Stat. Phys. Plasmas Fluids Relat. Interdiscip. Top.* **54,** 5538–5560.
27. Cassimeris, L., Gard, D., Tran, P. T. & Erickson, H. P. (2001) *J. Cell Sci.* **114,** 3025–3033.